ARL-TR-8396 ● JUNE 2018

US Army Research Laboratory

Single-Particle SERS Enhancement with Optimized Gold-Nanostar Morphologies

by Thomas Li, Yusong Choi, and Mark H Griep

NOTICES

Disclaimers

The findings in this report are not to be construed as an official Department of the Army position unless so designated by other authorized documents.

Citation of manufacturer's or trade names does not constitute an official endorsement or approval of the use thereof.

Destroy this report when it is no longer needed. Do not return it to the originator.

ARL-TR-8396 ● JUN 2018

US Army Research Laboratory

Single-Particle SERS Enhancement with Optimized Gold-Nanostar Morphologies

by Thomas Li
Oak Ridge Institute for Science and Education (ORISE)

Yusong Choi
Engineer and Scientist Exchange Program (ESEP)

Mark H Griep
Weapons and Materials Research Directorate, ARL

REPORT DOCUMENTATION PAGE

Form Approved
OMB No. 0704-0188

1. REPORT DATE *(DD-MM-YYYY)*	2. REPORT TYPE	3. DATES COVERED (From - To)
June 2018	Technical Report	June 2017–December 2017

4. TITLE AND SUBTITLE
Single-Particle SERS Enhancement with Optimized Gold-Nanostar Morphologies

5a. CONTRACT NUMBER

5b. GRANT NUMBER

5c. PROGRAM ELEMENT NUMBER

6. AUTHOR(S)
Thomas Li, Yusong Choi, and Mark H Griep

5d. PROJECT NUMBER

5e. TASK NUMBER

5f. WORK UNIT NUMBER

7. PERFORMING ORGANIZATION NAME(S) AND ADDRESS(ES)
US Army Research Laboratory
ATTN: RDRL-WMM-G
Aberdeen Proving Ground, MD 21005-5069

8. PERFORMING ORGANIZATION REPORT NUMBER
ARL-TR-8396

9. SPONSORING/MONITORING AGENCY NAME(S) AND ADDRESS(ES)

10. SPONSOR/MONITOR'S ACRONYM(S)

11. SPONSOR/MONITOR'S REPORT NUMBER(S)

12. DISTRIBUTION/AVAILABILITY STATEMENT
Approved for public release; distribution is unlimited.

13. SUPPLEMENTARY NOTES

14. ABSTRACT
The field of plasmonic nano-additives is expanding beyond the targeted synthesis of energy-tuned absorption materials toward the development of additive structures that efficiently translate the absorbed energy into a material response. In this work, the methodology to create gold nanostars with tailored extrusion features is optimized through a detailed investigation on the impact of each reaction chemical on the resulting structure morphology. Key elements including silver nitrate, ascorbic acid, and chloroauric acid concentrations are isolated to control nanostar tip length, symmetry, and quantity. Utilizing the optimized gold-nanostar structure, a Raman tag sensitive to the plasmon field is integrated into nanostar structure at defined locations to isolate the regions of maximal plasmon intensity. The reporter molecule demonstrated an 18-fold enhancement in Raman signal intensity when adhered to the nanostar protrusions over other locations on the particle, isolating the area of highest plasmon intensity at the nanostar tips.

15. SUBJECT TERMS
gold nanostars, surface-enhanced Raman spectroscopy, SERS, plasmonics, plasmonic energy transfer

16. SECURITY CLASSIFICATION OF:			17. LIMITATION OF ABSTRACT	18. NUMBER OF PAGES	19a. NAME OF RESPONSIBLE PERSON
a. REPORT	b. ABSTRACT	c. THIS PAGE			Mark H Griep
Unclassified	Unclassified	Unclassified	UU	19	19b. TELEPHONE NUMBER (Include area code) 410-306-4953

Contents

List of Figures

List of Tables

Acknowledgments

This research was supported in part by an appointment to the Postgraduate Research Participation Program at the US Army Research Laboratory (ARL) administered by the Oak Ridge Institute for Science and Education through an interagency agreement between the US Department of Energy and ARL.

1. Introduction

Plasmonic nanomaterials have been the focus of intense study in recent years, with widespread, realized application areas including sensing,[1] photothermal therapy,[2] bioimaging,[3] photocatalysts,[4] optical lenses,[5,6] thermal history measurements,[7] and polymer nanocomposites.[8,9] The extensive application potential results from the unique light–matter interactions with tailored plasmonic particles and structures. At a size scale smaller than the wavelength of light, metal nanoparticles generate a localized surface plasmon resonance (SPR) upon electromagnetic (EM) irradiation, where the oscillating electric field of the incident light is in resonance with collective oscillation of the nanoparticle's electron cloud. The large oscillations of the electron cloud enhance the nanoparticle's effective absorption cross-sectional area, resulting in a photon-trapping area up to an order of magnitude larger than the base-particle dimensions.

Apart from an amplified optical-extinction coefficient, synthesis methodologies are available to tune the resonance peak across the ultraviolet (UV), visible (Vis), and near-infrared spectrum to tailor the materials' use in select energy regions. By inducing asymmetry in the nanomaterials' structure, the resonance band can be shifted to the desired location in the EM spectrum. Multiple asymmetric morphologies have been optimized to exploit this tunability including silver nanoplates (AgNPs),[10] gold nanorods,[11–13] gold nanostars (AuNSs),[8] hollow gold nanoshells,[14] and core-shell designs.[15,16] In the case of silver nanoplates, for example, the aspect ratio is based upon the ratio of plate thickness to plate diameter, with a high aspect ratio leading to a red-shifted resonance. For gold-based materials, such as nanorods, the asymmetric morphology results in two separate resonance peaks corresponding to the transverse and longitudinal SPR. The multiple resonance modes highlight the ability to manipulate the plasmonic field based on the particle structure, providing the opportunity to focus the intensity of the plasmon in select regions of the particle. Recent efforts have demonstrated the ability to utilize high-intensity plasmon fields to manipulate the local environment and transfer energy to adjacent molecules.

In this work, methods to precisely tailor the morphology of AuNSs and locate/optimize the maximal plasmonic energy-transfer regions are reported. The sharp protrusions on AuNSs have been shown to serve as focusing points for plasmon energy[17]; thus, optimization of the synthesis protocol will allow for tailoring of the plasmon-focusing effects through design of the protruding spikes. With the creation of the focused-plasmon points, the energy can be utilized to enhance the Raman signature of attached molecules without the need of a precise

nanogap between adjacent plasmonic structures as used in traditional surface enhanced Raman spectroscopy (SERS) approaches.[18,19]

2. Experimental Procedure

2.1 Materials

Unless specified, all chemicals were purchased from Sigma-Aldrich (St Louis, Missouri) and used without further purification. Primary chemicals include silver nitrate ($AgNO_3$), trisodium citrate (Na-Cit), sodium borohydride ($NaBH_4$), hydrochloric acid (HCl), chloroauric acid ($HAuCl_4$), ascorbic acid (AA), poly(ethylene glycol) methyl ether thiol (mPEG-SH), copper (II) chloride, sodium dodecyl sulfate, sodium hydroxide, and hydroxylamine hydrochloride. All solutions were prepared in Milli-Q water.

2.2 Citrate-Stabilized Ag-Nanoseed Synthesis

Citrate-stabilized silver nanoseeds were synthesized following the previously reported method.[20] In a large beaker, a 200-mL solution of AgNO3 (0.25 mM) and Na-Cit (0.25 mM) was prepared. This solution was stirred for 30 min following the addition of 6 mL of NaBH4 (10 mM). The solution was left undisturbed overnight and stored at room temperature until use.

2.3 Ag-Core AuNS Synthesis

AuNSs with silver cores were synthesized following the previously reported method.[21] The previously synthesized Ag nanoseeds (0.75 mL) was added to 9 mL of distilled deionized (DDI) water and stirred for 1 min. Next, 7.5 μL of 100-mM HCl was added followed by 1 ml of 2.5-mM $HAuCl_4$. Afterward, 60 μL of 10-mM $AgNO_3$ and 50 μL of 100-mM AA were added simultaneously under vigorous stirring. After 1 min, 20 μL of 2-mM mPEG-SH was added and the solution was stirred for 30 min. The nanostars were then collected via centrifugation at 8,500 xg, washed thrice in water, and resuspended in 10 mL of DDI water.

Modifications of this procedure were made to create 10 variations of nanostars toward optimizing the morphology for enhance protrusions. These modifications were halving or doubling the amounts of the following: Ag nanoseeds, HCl, $HAuCl_4$, $AgNO_3$, and AA. Each modification was made noncongruent with other modifications, with Table 1 outlining the chemicals utilized for each sample.

2.4 Transmission Electron Microscopy (TEM) Grid Preparation

Transmission electron microscopy (TEM) was used to analyze the structural properties of the nanostars. TEM grids were prepared with copper oxide (CuO_2)–Au–Ag nanostars and Au–Ag nanostars. A 3-µL drop of the Au–Ag nanostars solution was placed on the TEM grid. The water was allowed to slowly evaporate at room temperature. A drop of the CuO_2–Au–Ag-nanostars solution was placed on the TEM grid. The ethanol was allowed to slowly evaporate at room temperature. Structural characterization was obtained by TEM on a Jeol 2100 (Peabody, Massachusetts) at 200 KeV.

2.5 Single Particles SERS Synthesis

Two sets of AuNSs were synthesized with rhodamine 6g (Rh6G) for Raman analysis. A total of 50µl of 0.1-mM Rh6G was added to the samples at select points in the synthesis procedure to isolate the Raman tag into specified locations within the particle.

3. Results

3.1 Morphology Optimization

Alterations to the selected parameters described in Table 1 produced the AuNSs shown in the TEM images of Figs. 1 and 2. Initial image analysis demonstrates an enhancement of the star tips' density when the HCl concentration was doubled versus control. Additionally, an increased symmetric formation correlates with an increase in HAuCl4 concentration. The same symmetric formation was also noted when the ascorbic-acid concentration was halved. Furthermore, halving the concentration of AgNO3 produced a higher degree of star tips but not to the degree as seen when the HCl was doubled.

Table 1 Reactants used for the preparation of sample variants, with yellow-highlighted regions corresponding to key alteration from control

	Control	Sample 1	Sample 2	Sample 3	Sample 4	Sample 5	Sample 6	Sample 7	Sample 8	Sample 9	Sample 10
Ag NPs	0.75 mL	0.375 mL	1.5 mL	0.75 mL	0.75 mL	0.75 mL	0.75 mL	0.75 mL	0.75 mL	0.75 mL	0.75 mL
DDI	9 mL	9 mL	9 mL	9 mL	9 mL	9 mL	9 mL	9 mL	9 mL	9 mL	9 mL
0.1 M HCl	7.5 µL	7.5 µL	7.5 µL	3.75 µL	15 µL	7.5 µL	7.5 µL	7.5 µL	7.5 µL	7.5 µL	7.5 µL
2.5 mM HAuCl4	1 mL	1 mL	1 mL	1 mL	1 mL	0.5 mL	2 mL	1 mL	1 mL	1 mL	1 mL
100 mM AA	50 µL	50 µL	50 µL	50 µL	50 µL	50 µL	50 µL	25 µL	100 µL	50 µL	50 µL
10 mM AgNO3	60 µL	60 µL	60 µL	60 µL	60 µL	60 µL	60 µL	60 µL	60 µL	30 µL	120 µL
2 mM mPEG-SH	20 µL	20 µL	20 µL	20 µL	20 µL	20 µL	20 µL	20 µL	20 µL	20 µL	20 µL

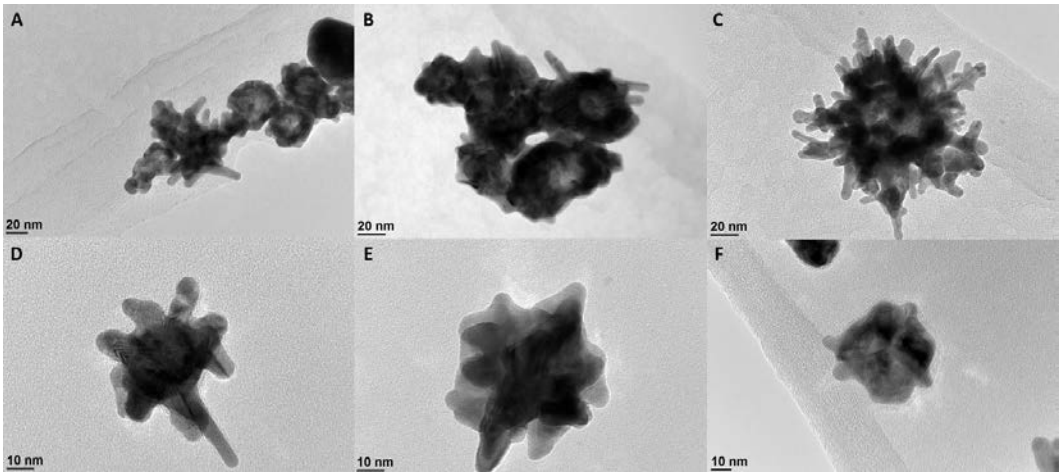

Fig. 1 With A) as unaltered control, TEM images of synthesized AuNS resulting from test-reaction conditions focused on *doubled* concentrations of B) Ag nanoparticles, C) 0.1-M HCl, D) 2.5-mM HAuCL4, E) 100-mM ascorbic acid, and F) 10-mM AgNO3

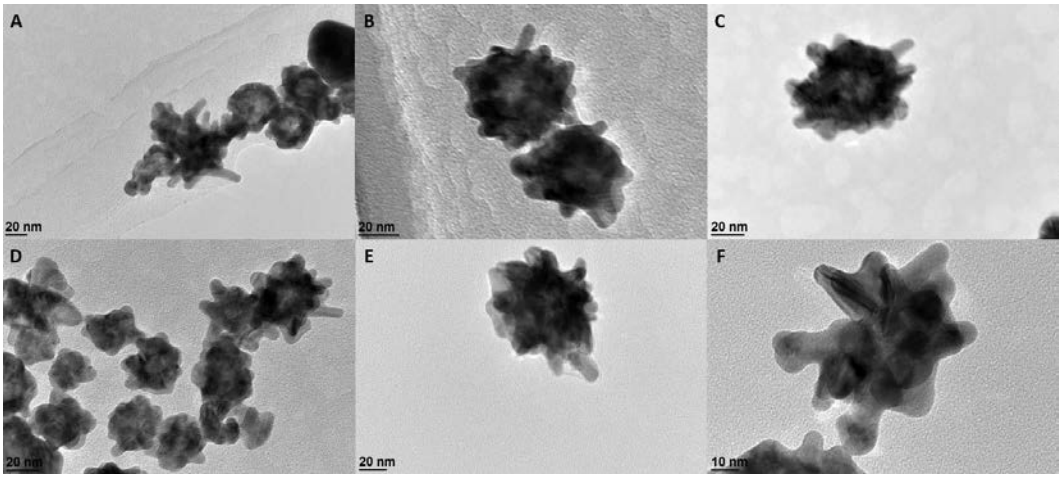

Fig. 2 With A) as unaltered control, TEM images of synthesized AuNS resulting from test-reaction conditions focused on *halved* concentrations of B) Ag nanoparticles, C) 0.1-M HCl, D) 2.5-mM HAuCL4, E) 100-mM ascorbic acid, and F) 10-mM AgNO3

To analyze the impact of morphology on the resulting plasmonic absorption properties, UV–Vis spectroscopy was measured from 350 nm to 1300 nm as shown in Fig. 3. Figure 4 isolates the absorbance properties of each altered chemical species with respect to the control. The control sample shows a saturation peak of 604 nm and a normalized range from 534 nm to 705 nm.

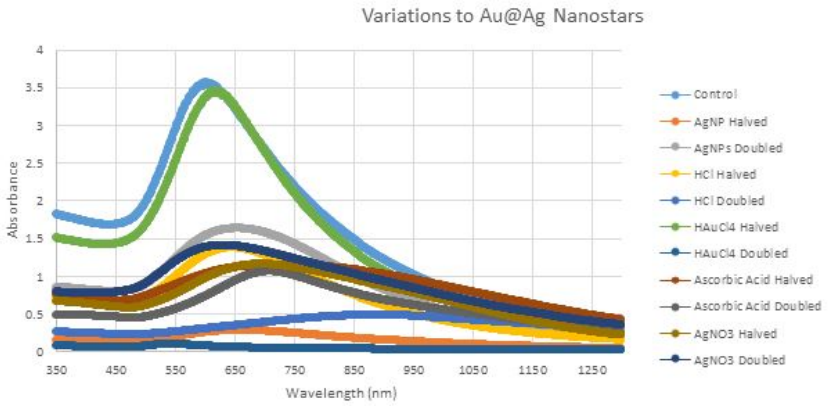

Fig. 3 Overall UV–Vis absorption spectra of prepared AuNS samples

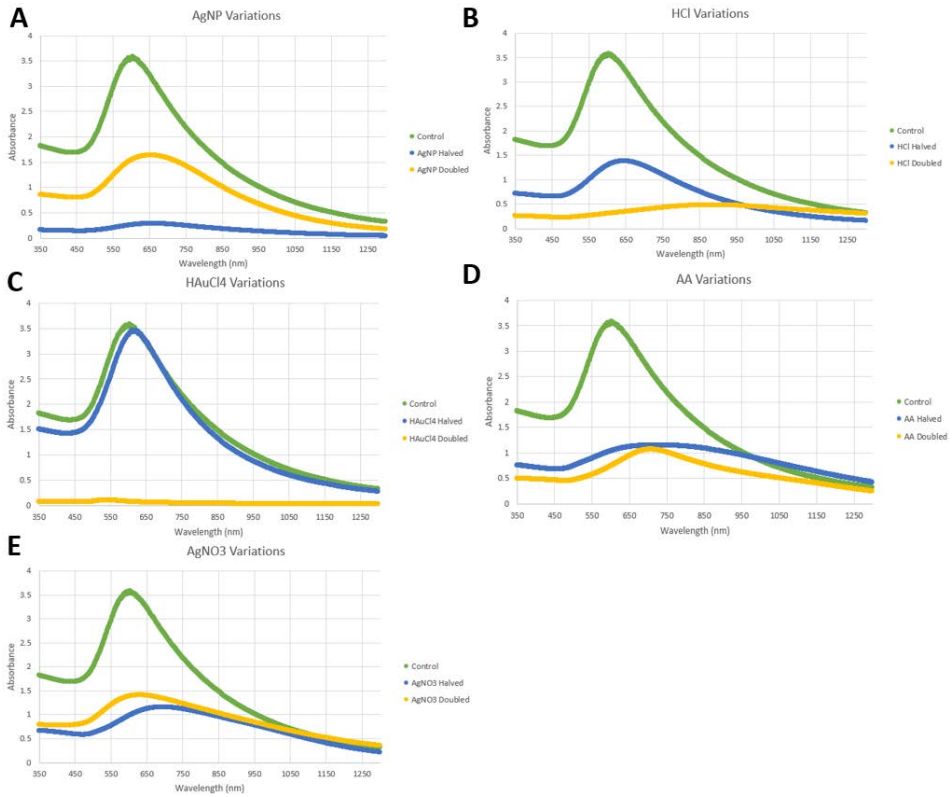

Fig. 4 Isolated UV–Vis absorption with targeted synthesis-parameter adjustments of A) AgNP, B) 0.1-M HCl, C), 2.5-mM HAuCL4, D) 100-mM AA, and E) 10-mM AgNO3; halved parameters are blue, doubled parameters are yellow, and green is control

The normalized ranges are provided in Table 2 with the samples' names matching those in Table 1. It was noted the majority of the samples had the same wavelength range as those of the control yet the absorbance levels were reduced, correlating to a lower concentration of plasmonic materials. A comparison with the TEM images in Figs. 1 and 2 shows a greater dispersity of nanostars with defined tips than those

of the control. In conjunction with the visual analysis from the TEM, it can be concluded the number of tips shifts the absorbance range with the enhanced star-tip density.

Table 2 Normalized resonance peaks and absorption range of prepared samples; sample (S) names correspond with the solution variation in Table 1

Sample	Lower Wavelegth (nm)	Saturation Peak (nm)	Upper Wavelength (nm)	Wavelength Range (nm)
Control	534	604	705	171
S1	552	658	797	245
S2	547	653	801	254
S3	552	644	772	220
S4	647	881	1187	540
S5	545	611	719	174
S6	509	540	566	57
S7	558	728	970	412
S8	604	707	860	256
S9	573	694	899	326
S10	530	633	820	290

3.2 Single-Particle SERS

To localize the regions of maximal plasmonic field strength within the multilayered nanostar structure, a plasmonically enhanced sensitizer was integrated at specific stages of the material synthesis. An Rh6G was used as the sensitizer due to its previously demonstrated utility as a SERS probe. As shown in Fig. 5, the Rh6G molecule was adsorbed with four distinct configurations to isolate plasmonic strength at the AgNP surface, AgNP–AuNS interface, AuNS protrusions, and combined interface/protrusions. With these configurations the Raman enhancement can be isolated to specific regions within the hybrid particle to determine if the AgNP core, Ag–Au interface, or AuNS protrusions yield the strongest plasmon field intensities.

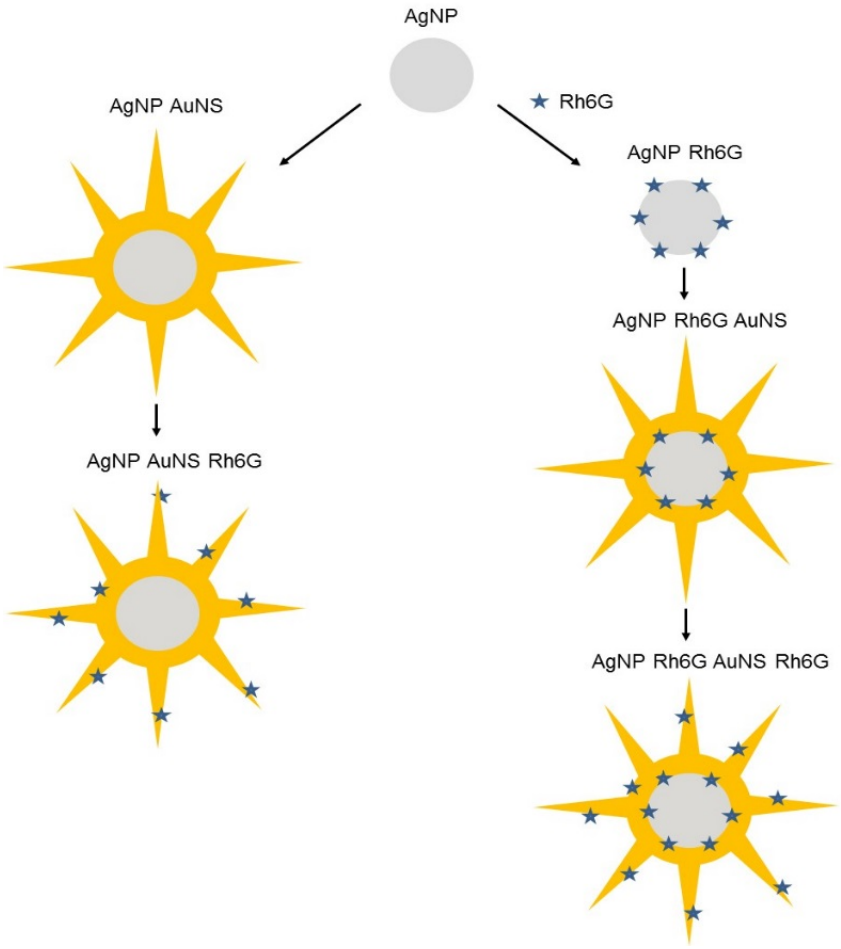

Fig. 5 Schematic of synthesis steps to create single-particle SERS enhancement

With the hybridized particles prepared as described in Fig. 5, Raman analysis was performed to analyze the Rh6G SERS signal on each construct. As shown in Fig. 6, a marked difference in signal intensities is evident. With the Rh6G control, this Raman signal is from a concentrated deposition of the reporter molecule whereas the presence of Rh6G hybridized onto the nanoparticle hybrids will be of substantially lower concentration. All hybridized nanoparticles were prepared to the same concentration for Raman analysis. Although the Rh6G control is measured from a higher concentration of reporters, the signal enhancement resulting from the AuNS is clear. Compared to the Rh6G control, AuNS structures with Rh6G absorbed to the protrusions resulted in an 18-fold signal enhancement. The samples attaching Rh6G at the AgNP surface and AgNP–AuNS interface demonstrated no clear enhancement above control, although SERS activity cannot be ruled out since the Rh6G concentration is lower in the hybridized samples. Comparing the two samples, which adhered Rh6G at the nanostar protrusions, it is interesting to note the addition of Rh6G at the AuNP–AuNS interface reduced the subsequent SERS performance, reducing the signal enhancement to 12-fold over control. It is likely

the presence of Rh6G on the AgNP surface prior to AuNS growth hindered subsequent star formation, limiting subsequent SERS activity. This likelihood notwithstanding, the results demonstrate the primary region on the AuNS construct for enhanced plasmon field strength is associated with the gold protrusions from the particle core.

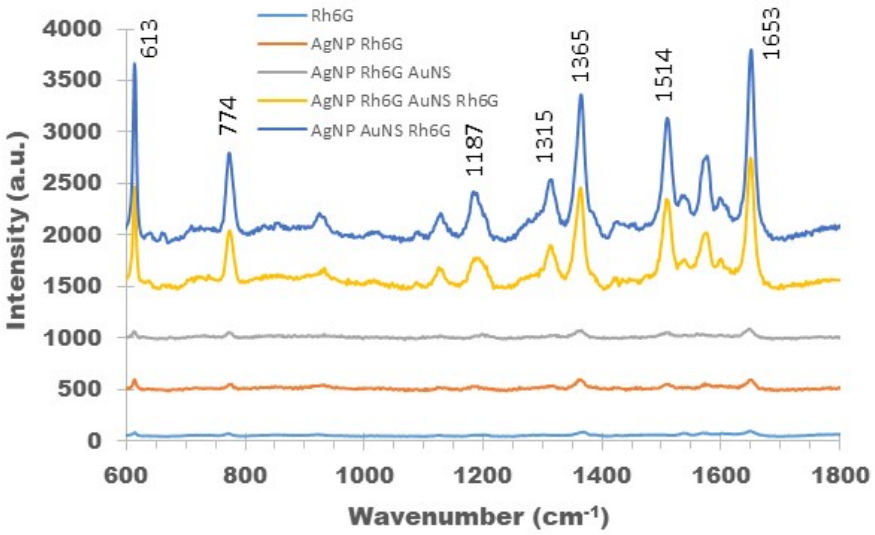

Fig. 6 Raman signal generated from Rh6G in control state and when attached in specified regions of AgNP–AuNS core-shell particle

4. Conclusions

In this work we analyzed the impact of each chemical component involved in AuNS synthesis on the particles' final morphology. By isolating the individual reactants and varying their respective concentrations to 0.5 and 2 times the molar concentrations utilized in standard protocols, key synthesis variables were identified. In particular, it was found the morphology of the nanostars can be directly altered with slight variations in the amount of $AgNO_3$ and HCl used. An increase to the number of tips was achieved by either reducing the $AgNO_3$ or providing an excess of HCl in the reaction. It was also found that amount of HAuCl4 could hinder nanostar formation when applied in excess of the noted standard conditions. Utilizing the produced AuNS particles, identification of the particle regions associated with maximal plasmonic activity was achieved. Incorporating the Rh6G Raman tag on the AuNS protrusions yielded an 18-fold increase in Raman signal intensity over control and when Rh6G was on the AgNP core and Ag–Au interface. Therefore, optimizing the synthesis procedure to allow precise control over the AuNS-protrusion features is a critical step toward optimizing AuNS particles toward select plasmonic applications.

5. References

1. Fu LS, Wang WS, Xu CY, Li Y, Zhen L. Design, fabrication and characterization of pressure-responsive films based on the orientation dependence of plasmonic properties of Ag@Au nanoplates. Sci Rep. 2017;7(1676):1–9.

2. Dickerson EB, Dreaden EC, Huang X, El-Sayed IH, Chu H, Pushpanketh S, McDonald JF, El-Sayed MA. Gold nanorod assisted near-infrared plasmonic photothermal therapy (PPTT) of squamous cell carcinoma in mice. Can Lett. 2008;269(1):57–66.

3. Hore MJA, Composto RJ. Functional polymer nanocomposites enhanced by nanorods. Macromolecules. 2014;47(3):875–887.

4. Ray C, Pal T. Recent advances of metal-metal oxide nanocomposites and their tailored nanostructures in numerous catalytic applications. J Mat Chem A. 2017;5(20):9465–9487.

5. Tritschler U, Zlotnikov I, Keckeis P, Schlaad H, Cölfen H. Optical properties of self-organized gold nanorod-polymer hybrid films. Langmuir. 2014;30(46):13781–13790.

6. Li L, Sun L, Gomez-Diaz JS, Hogan NL, Lu P, Khatkhatay F, Zhang W, Jian J, Huang J, Su Q, et al. Self-assembled epitaxial Au-oxide vertically aligned nanocomposites for nanoscale metamaterials. Nano Lett. 2016;16(6):3936–3943.

7. Wang Y-C, Lu L, Gunasekaran S. Biopolymer/gold nanoparticles composite plasmonic thermal history indicator to monitor quality and safety of perishable bioproducts. Biosen Bioel. 2017;92:109–116.

8. Boyne DA, Orlicki JA, Walck SD, Savage AM, Li T, Griep MH. Plasmonic gold nanostars as optical nano-additives for injection molded polymer composites. Nanotechnology. 2017;28(40):1–8.

9. Boyne DA, Savage AM, Griep MH, Beyer FL, Orlicki JA. Process induced alignment of gold nano-rods (GNRs) in thermoplastic polymer composites with tailored optical properties. Polymer. 2017;110:250–259.

10. Boyne DA, Orlicki JA, Griep MH. Plasmonic nano-additives for polymer composites: preservation of tailored functionality, nanotechnology. IEEE-NANO 2017. Proceedings of the 17th IEEE International Conference on Nanotechnology; 2017 Jul 25–28; Pittsburgh, PA. IEEE; 2017. p. 881–884.

11. Boyne DA, Chipara AC, Giri L, Griep MH. Stabilization of gold nano-rods (GNRs) in aqueous and organic environments by select surface functionalization. Aberdeen Proving Ground (MD): Army Research Laboratory (US); 2016 Jan. Report No.: ARL-TR-7581.

12. Boyne DA, Chipara AC, Griep MH. Transverse axis morphological control for tailored gold nanorod (GNR) synthesis. RSC Adv. 2016;6(68):63634–63641.

13. Williams MG, Boyne DA, Griep MH. Rapid synthesis of high purity gold nanorods via microwave irradiation. Mat Res Exp. 2017;4(3):1–7.

14. Mackay RA, Giri L, Karna SP, Griep MH. Galvanic synthesis of hollow gold nanoshells. Aberdeen Proving Ground (MD): Army Research Laboratory (US); 2015 Feb. Report No.: ARL-TR-7219.

15. Boyne DA, Griep MH. Decorated core-shell architectures: influence of the dimensional properties on hybrid resonances. Plasmonics. 2017;1–8.

16. Williams MG, Boyne DA, Tran N, Bujanda AA, Griep MH. Aberdeen Proving Ground (MD): Army Research Laboratory (US); 2017. Report No.: ARL-TR-8182.

17. Hao F, Nehl CL, Hafner JH, Nordlander P. Plasmon resonances of a gold nanostar. Nano Lett. 2007;7(3):729–732.

18. Michota A, Bukowska J. Surface-enhanced Raman scattering (SERS) of 4-mercaptobenzoic acid on silver and gold substrates. J Raman Spectro. 2003;34(1):21–25.

19. Zhao B, Shen J, Chen S, Wang D, Li F, Mathur S, Song S, Fan C. Gold nanostructures encoded by non-fluorescent small molecules in polyA-mediated nanogaps as universal SERS nanotags for recognizing various bioactive molecules. Chem Sci. 2014;5(11):4460–4466.

20. Doty RC, Tshikhudo TR, Brust M, Fernig DG. Extremely stable water-soluble Ag nanoparticles. Chem Mat. 2005;17(18):4630–4635.

21. Zeng L, Pan Y, Wang S, Wang X, Zhao X, Ren W, Lu G, Wu A. Raman reporter-coupled Ag core@Au shell nanostars for in vivo improved surface enhanced Raman scattering imaging and near-infrared triggered photothermal therapy in breast cancers. ACS App Mat Inter. 2015;7(30):16781–16791.

List of Symbols, Acronyms, and Abbreviations

AA	ascorbic acid
Ag	silver
$AgNO_3$	silver nitrate
AgNP	silver nanoplate
Au	gold
AuNS	gold nanostar
CuO_2	copper oxide
DDI	distilled deionized
EM	electromagnetic
$HAuCl_4$	chloroauric acid
HCl	hydrochloric acid
mPEG-SH	poly(ethylene glycol) methyl ether thiol
Na-Cit	sodium citrate
$NaBH_4$	sodium borohydride
Rh6G	rhodamine 6G
S	sample
SERS	surface enhanced Raman spectroscopy
SPR	surface plasmon resonance
TEM	transmission electron microscope
UV	ultraviolet
Vis	visible

1 (PDF)	DEFENSE TECHNICAL INFORMATION CTR DTIC OCA
2 (PDF)	DIR ARL IMAL HRA RECORDS MGMT RDRL DCL TECH LIB
1 (PDF)	GOVT PRINTG OFC A MALHOTRA
4 (PDF)	ARL RDRL WMM A J SANDS RDRL WMM G M GRIEP J LENHART T LI